Supplementary Information

Molybdenum Nanoclusters as Potent Antioxidants for the Treatment of Osteoarthritis

Hui Yang[a, 1], Wei Liu[b, 1], Renwei Wang[a,1], Binbin Zhang[a], Wenge Wang[a], Jianlin Wu [a], Peng Jiang[a], Yandong Zhao[a], Xu Liang[a], Xiaotong Feng[c, *], Huawei Zhang[a, *]

[a]Department of Orthopedic, Lin Fen Central Hospital Affiliated to ChangZhi Medical College, 041000, China.

[b]Department of Orthopedic, The Fifth Affiliated Hospital, Sun Yat-sen University, Zhuhai, Guangdong Province 519000, China.

[c]Emergency department, Zhuhai Center for Chronic Disease Control & Zhuhai Third People' s Hospital, Zhuhai 519000, PR China.

[1]Hui Yang, Wei Liu and Renwei Wang are co-first authors.

* Corresponding author E-mail addresses: xiaotongfeng0804 (Xiaotong Feng), zhanghuawei1218@163.com (Huawei Zhang).

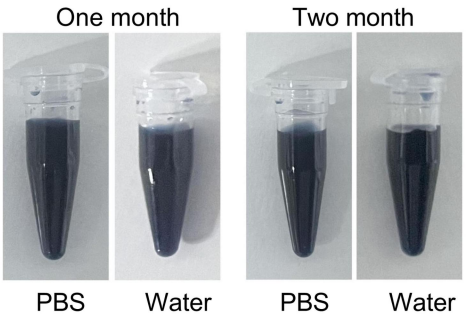

Fig. S1. Photograph of MNs dispersed in PBS and water, and characterization of their stability.

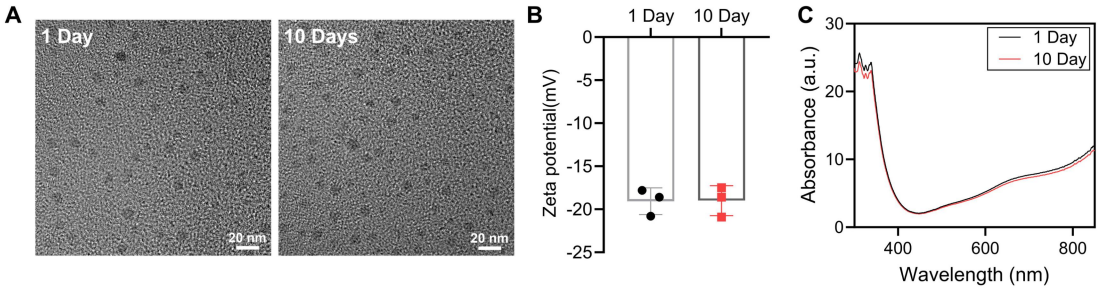

Fig. S2. (A) TEM images of the nanoparticles after storage for 1 day and 10 days, showing no obvious morphological changes. Scale bar: 20 nm. (B) Zeta potential of the nanoparticles measured after 1 day and 10 days of storage, indicating stable surface charge over time. (C) UV–vis absorption measurements of the nanoparticles measured after 1 day and 10 days of storage.

Fig. S3. Characterization the of MNs. The MNs can be synthesized in a large-scale method, photograph of the as-made MNs showing the product.

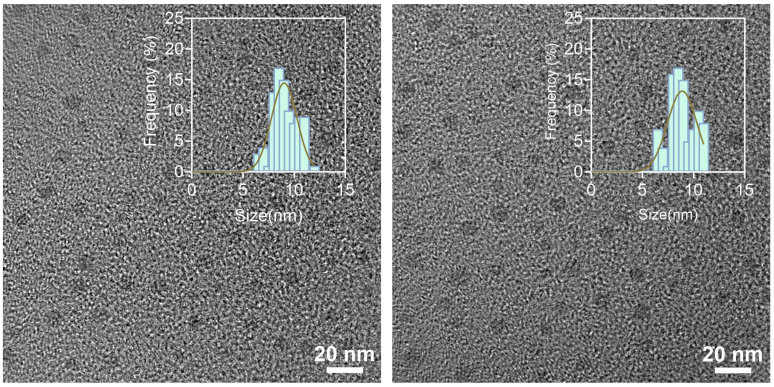

Fig. S4. TEM images and corresponding particle size distributions of materials obtained from two independent gram-scale syntheses (Batch 1 and Batch 2), demonstrating good batch-to-batch reproducibility.

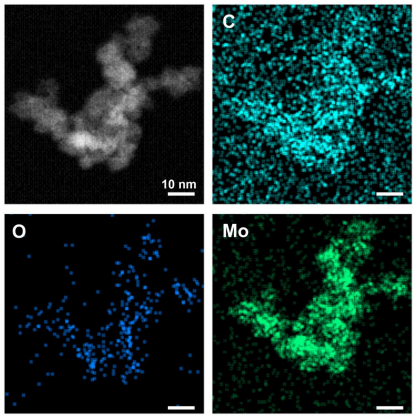

Fig. S5. Characterization of MNs. EDS measures the presence of all expected essential chemical elements (Mo, O, and C) of MNs.

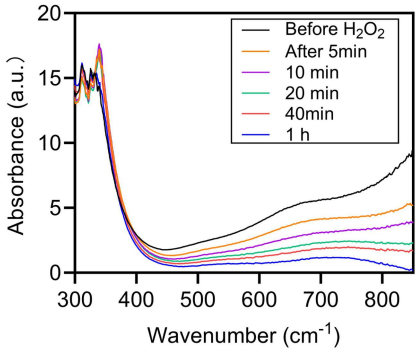

Fig. S6. Time-dependent UV-absorbance curve of MNs.

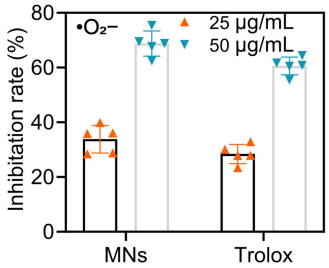

Fig. S7. The ROS scavenging efficiency of MNs and Trolox was compared across various concentrations.

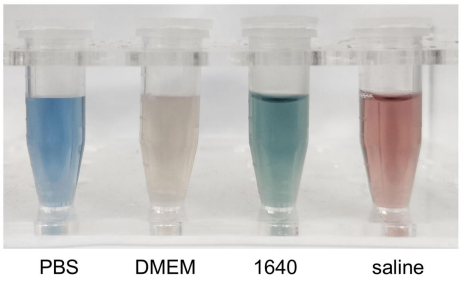

Fig. S8. Photographs of MNs in different solutions.

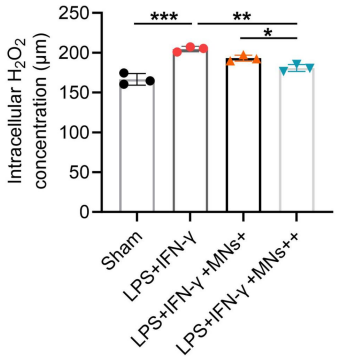

Fig. S9. Quantification of intracellular H_2O_2 levels in RAW 264.7 cells across different experimental groups. Data represent mean ± SD (n = 3). *$p < 0.05$, **$p < 0.01$, ***$p < 0.001$.

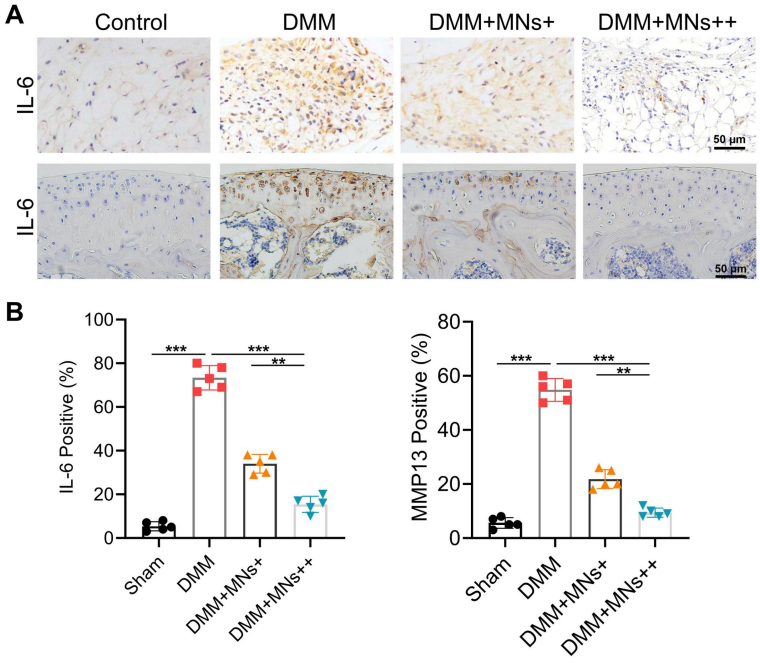

Fig. S10. Immunohistochemical staining of synovium and articular cartilage. (A) IL-6 of synovium. (B) IL-6 in articular cartilage. (C-D) Quantitative analysis of IL-6 in synovium and in articular cartilage. Scale bar: 50 μm. Data represent mean ± SD (n = 3). *$p < 0.05$, **$p < 0.01$, ***$p < 0.001$.

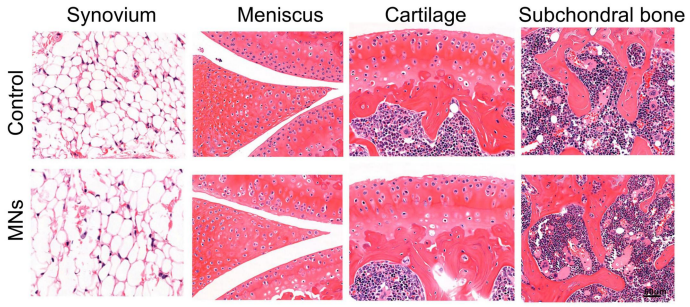

Fig. S11. Histological evaluation of local toxicity in vivo. Representative H&E-stained images of mouse knee joints after 2 months of treatment with control or MNs. Scale bar: 50 μm.

Table S1. Mouse real-time PCR primer sequences used in this study.

Genes	Primer	Primer sequence (5′ –3′)
iNOS	Forward	TTGGGAGGAGAAGGCGTTTG
	Reverse	TCCACTGCCCCAGTTTTTGA
Arg-1	Forward	CGGCAGTGGCTTTAACCTTG
	Reverse	TTGGGAGGAGAAGGCGTTTG
β-actin	Forward	GCTGTGCTATGTTGCTCTAG
	Reverse	CGCTCGTTGCCAATAGTG
ACAN	Forward	GTGGAGCCGTGTTTCCAAG
	Reverse	AGATGCTGTTGACTCGAACCT
Col2a1	Forward	GGGAATGTCCTCTGCGATGAC
	Reverse	GAAGGGGATCTCGGGGTTG
SOX-9	Forward	CGGAACAGACTCACATCTCTCC
	Reverse	GCTTGCACGTCGGTTTTGG
Adamts-5	Forward	GGAGCGAGGCCATTTACAAC
	Reverse	CGTAGACAAGGTAGCCCACTTT
MMP-13	Forward	GGAGCGAGGCCATTTACAAC
	Reverse	CGTAGACAAGGTAGCCCACTTT
COX-2	Forward	GATGACGAGCGACTGTTCCA
	Reverse	CAGCGGATGCCAGTGATAGA